Chemical Engineering Journal 281 (2015) 312–321

Contents lists available at ScienceDirect

Chemical Engineering Journal

journal homepage: www.elsevier.com/locate/cej

Critical process parameters and their interactions on the continuous hydrothermal synthesis of ironoxide nanoparticles

Brett Kriedemann, Veruscha Fester *

Cape Peninsula University of Technology, Faculty of Engineering, P.O. Box 652, Cape Town 8000, South Africa

HIGHLIGHTS

- Iron oxide nanoparticles were synthesized using continuous hydrothermal synthesis.
- The critical process parameters were evaluated on particle characteristics.
- A factorial trial was conducted and interactions between parameters were evaluated.
- Critical process interactions: temperature and flow rate and concentration and temperature.

ARTICLE INFO

Article history:
Received 26 January 2015
Received in revised form 28 May 2015
Accepted 29 May 2015
Available online 16 June 2015

Keywords:
Continuous hydrothermal synthesis
Hematite
Nanoparticles
Factorial design
Interaction
Operating parameters

ABSTRACT

Conflicting reports exist about the critical process conditions for continuous hydrothermal synthesis of metal oxide nanopowders and are often accredited to the inability to isolate the effect of various operating parameters and the complexity of particle formation. In this study, an investigation was conducted on the effect of process parameters and their interactions during the continuous hydrothermal synthesis of hematite (α-Fe_2O_3) nanoparticles. Utilizing a 3-level, 3-factor Box-Behnken factorial design, the individual operating parameters (concentration, temperature and flow rate) and their interactions were evaluated. The interactions between operating parameters were found to be significant, especially in the case of temperature and concentration. The temperature and concentration were found to interact revealing three different trends on the average particle size, offering a solution to conflicting reports in the literature. The temperature was also observed to interact favourably with the flow rate, presenting a method of increasing the particle yield and relative crystallinity, with little change in average particle size or particle size distribution. This knowledge will prove invaluable for the design of future experiments in CHS.

1. Introduction

In current times, a fundamental aspect of nanotechnology research is the development of reliable synthesis protocols for nano structured materials over a range of chemical compositions, shapes and sizes [1]. As the physical and chemical properties of nanoscale materials are strongly dependent on their size, size distribution, and structures, it is essential to maintain control over particle characteristics [2]. Teja and Koh [3] reviewed numerous synthesis strategies for three different types of iron oxide nanoparticles, and proposed that continuous hydrothermal synthesis (CHS) was most promising for process control, particle characteristics control and plant scalability. Although high quality particles with a narrow size distribution have been produced via the CHS method, Xu [4] stressed that the effects of operating parameters are not well understood, often citing conflicting reports in the literature. One of these uncertain parameters in CHS is the effect of temperature on particle size, where Hao and Teja [5] reported that temperature has no evident effect on the size of their iron oxide nanoparticles, while Xu and Teja [6] identified that particle size increased with increasing temperature. On the contrary, it was shown by Hakuta et al. [7] that their ceria particles decreased in size along with an increase in temperature.

Numerous authors have studied the effects of isolated operating parameters in CHS, such as concentration [5,6,8] reaction temperature [4,9], pressure [10], residence time [5,6,11] and pH [12]. Yet Cote et al. [12] identified that operating parameters in CHS are rather complex and difficult to isolate. One such example is that of temperature. When the temperature increases, it changes the fluid density and viscosity and hence the reaction rate and residence time. The resulting affect is a change in particle growth,

* Corresponding author. Tel.: +27 214603055.
E-mail addresses: brettkried@gmail.com (B. Kriedemann), festerv@cput.ac.za (V. Fester).

http://dx.doi.org/10.1016/j.cej.2015.05.115
1385-8947/

mixing characteristics and reaction time. As the evaluation of parameters through isolation appears to be feeble, a new technique was required. A more appealing approach was identified by Aimable et al. [13]. They used a factorial design to study the effect of operating parameters on the particle characteristics of $BaZrO_3$ powders, which used a set of statistical experiments to analyze the system as a whole. The factorial design was deemed successful, highlighting the temperature and NaOH concentration as having the largest influence on APS. However, the interactions between parameters were not reported.

Although the dependence of particle characteristics on the variation of operating parameters in CHS has been reported by several authors, a systematic study has yet to be performed to determine the critical process parameters and their interactions required for controlled growth of iron oxide nanoparticles. This study therefore focuses on the effect of operating parameters and their interactions on the resulting (a) average particle size (APS), (b) particle size distribution (PSD), (c) product yield (PY) and (d) relative crystallinity (RC) further aiding the controlled growth of metal oxide particles in CHS.

2. Experimental procedures

2.1. Experimental setup

Fig. 1 displays a schematic diagram of the continuous hydrothermal synthesis pilot plant constructed and commissioned in 2013 at the Cape Peninsula University of Technology (CPUT), Cape Town, South Africa. The CHS plant is capable of synthesizing numerous different types of metal oxide nanopowders, with this study focusing on hematite phase (α-Fe_2O_3) iron oxide. Other materials synthesized in this plant to date include TiO_2 and Ag nanoparticles.

The pilot plant depicted in Fig. 1, consists of two Isco Teledyne 260D high pressure syringe pump (water pump) set up in a duel system, for the constant delivery of supercritical water of up to 80 ml/min. A Milton Roy metallic diaphragm dosing pump (precursor pump) was used for pumping the precursor solution, which was capable of pumping corrosive fluids at up to 96.6 ml/min. Two plate heaters in series were used for heating the water feed, followed by a mixing tee, a reactor/crystallizer, a pipe in pipe cooling column and a back pressure regulator supplied by Tescom, leading to a sample collection vessel.

All tubing and fittings was supplied by Swagelok, where 3.175 mm O.D (1/8″) stainless steel 316 was used up to the mixing tee (except 6.35 mm OD tubing used in the plate heaters), followed by 6.35 mm OD (1/4″) stainless steel 316 tubing up to the collection vessel. The larger diameter tubing was used to avoid particle build up and potential clogging.

For process control, 4 temperature feedback controllers and 5 temperature indicators along with 9 thermocouples (5 inline and 3 clamp type) were supplied by Unitemp, R.S.A, for temperature monitoring and control. A pressure gauge was supplied by Swagelok, a pressure transducer was supplied from WIKA for

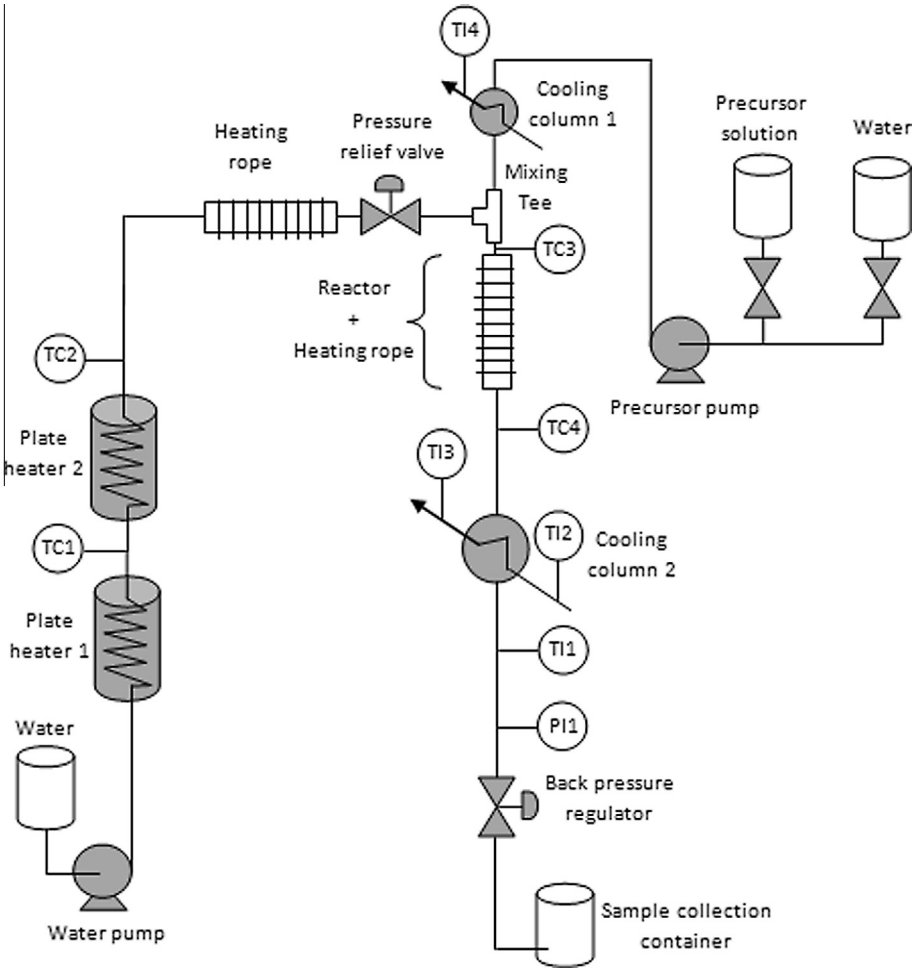

Fig. 1. Schematic diagram of CHS pilot plant constructed in 2013 at CPUT, Cape Town, South Africa.

pressure logging and a back pressure regulator was supplied by Tescom in order to monitor and control the pressure in the system. For safety purposes, a check valve was placed after each pump to prevent reverse flow, and a pressure release valve (set to fail at 320 atm) was installed in case of a pressure build up due to failure of the back pressure regulator.

2.2. Procedure and sample analysis

Ferric nitrate nonahydrate $Fe_2(NO)_3{\cdot}9H_2O$ (>98%) was supplied by Sigma–Aldrich and was the main constituent of the precursor solution makeup. Precursor solutions were prepared by mixing a given mass of the salt with deionized water in order to achieve a desired concentration. The pH of the solution was then adjusted to 1.8 by adding a 7 M solution of sodium hydroxide in a drop wise manner. A 100 ml of precursor solution was prepared for each experimental run. Once the CHS plant was running at steady state, and at the desired parameters for the experimental run, the precursor solution was pumped through the system and reacted in a 3:2 ratio of water to precursor. A 100 ml of product solution was collected at the end of the process and stored until separation. The particles were separated through centrifugation, with all experiments being centrifuged at 6000RPM for 5 min a minimum of 3 separate times, or until all particles were removed from suspension. The separated particles were then dispersed in deionized water and dried in an oven at 60 °C for 24 h. The yield of each experimental run was determined by weighing each empty Petri dish and full dish of particles after drying, using an electric balance accurate to 2 decimal places.

The retrieved powders were characterized using HRTEM and XRD. For HRTEM analysis, the iron oxide particles were dispersed in methanol and then sonicated for 20 min prior to being placed onto a copper-coated carbon grid. Once dried, the samples were placed inside the TEM and the surface morphology of the nanoscale crystals was studied using a Tecnai TF20 thermoionic HRTEM, equipped with a LaB6 filament and a Gatan GIF energy filter. The images were captured at 200 keV in bright field mode. Using Image J version 1.47 software, 200 (in some cases only 100) individual crystals were counted in order to determine the average particle size (APS) and particle size distribution (PSD). XRD characterization was performed using a Phillips PW 3830/40 generator with a PW 3710 mpd control X-ray diffraction system with Cu-Kα radiation (λ = 1.506 Å and the scan was conducted between 5° and 70° with a 0.02° step width. The crystal phase was then identified and evaluated using X'Pert Highscore (PANalytical. version 2.2c) software. The dominant phase in all samples was found to be hematite (α-Fe_2O_3) phase iron oxide, as shown by the reference pattern in Fig. 3. Pure hematite was obtained for Runs 5, 6, 9, 11 and 14. Additional peaks at 29, 38 and 48 2θ, not characteristic of the hematite phase and could not be matched to a reference pattern which took into account the starting materials. These were the first samples produced on the rig and samples could therefore not include any other impurities. Samples are currently examined to identify interesting phenomena associated due to the presence of these unknown peaks. An example of the diffraction patterns using a comparison of Run 1 and Run 5 is depicted in Fig. 2, showing the pure hematite phase in Run 5 and the unmatched peaks at 29, 38 and 48 2θ in Run 1.

The degree of crystallinity was determined using a method described by Gosh [14], where the sum of the peak intensities for were collected from the XRD data set and compared to the reference sample of the highest sum of peaks in this study. Therefore a relative crystallinity percentage could be obtained, converting the qualitative diffraction patterns into a quantitative crystallinity percentage. The relative crystallinity can be represented as follows in Eq. (1) [14]:

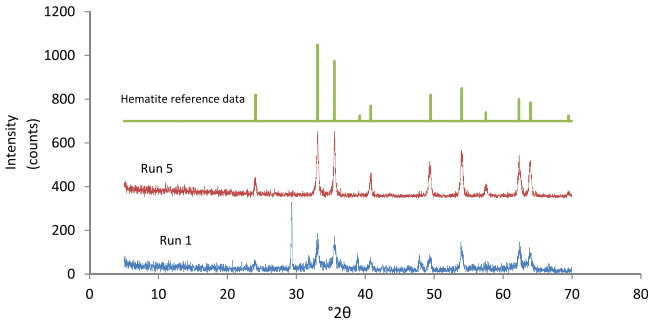

Fig. 2. Comparison of iron oxide diffraction patterns between Run 1, Run 5 and the Hematite reference pattern.

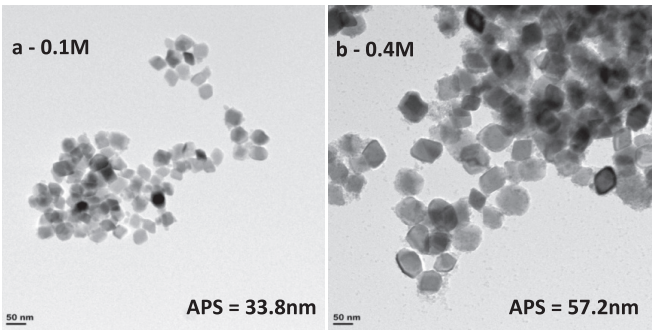

Fig. 3. HR TEM images of hematite nanoparticles synthesized at 300 °C and 50 ml/min flow rate with (a) Run 5–0.1 M and (b) Run 14–0.4 M.

Table 1
Variables in Box-Behnken factorial design.

Formulation variables	Levels used		
	Low	medium	high
Concentration (mol/dm^3)	0.1 (−1)	0.25 (0)	0.4 (+1)
Temperature (°C)	250 (−1)	300 (0)	350 (+1)
Flow rate (ml/min)	50 (−1)	75 (0)	100 (+1)

$$\text{Relative crystallinity} = \frac{\text{Sum of area under the XRD peaks of the product}}{\text{Sum of area under the XRD peaks of the reference sample}} \times 100 \quad (1)$$

2.3. Factorial trial design

A 3-level Box-Behnken factorial design was used to statistically analyse the parameters and parameter interactions using Stat Ease Design Expert V 7.0.0. The chosen parameters included precursor concentration, reaction temperature and flow rate (Table 1) and were evaluated by studying their interactions and effects on the resulting average particle size (APS), particle size distribution (PSD), relative crystallinity (RC) and product yield (PY). The results for each of the experimental runs are summarized in Table 2. For each of the responses, a correlation factor of significance was identified for each process parameter and a contribution percentage was determined for each parameter and parameter interaction. The contribution factor percentages were vital, not only for identifying possible parameter interactions but also for evaluating their influence on a given response.

Table 2
Factorial trial sample matrix: operating parameters and their respective particle characteristics.

Run	Concentration (mol/dm^3)	Temperature (°C)	Flow rate (ml/min)	Average particle size (nm)	Particle size distribution (CV%)	Relative crystallinity (%)	Product yield (%)
1	0.1	300	100	31.3	20.1	60.0	17.2
2	0.25	350	100	47.6	18.3	84.5	62.0
3	0.4	300	100	58.3*	24.7*	55.8	55.6
4	0.25	300	75	42.9	22.1	78.2	44.5
5	0.1	300	50	33.8	14.8	98.9	31.3
6	0.1	350	75	35.1	20.5	98.5	34.4
7	0.25	250	50	42.8	15.7	100	36.3
8	0.4	250	75	50.4*	22.6*	48.1	25.0
9	0.1	250	75	43.2*	26.4*	78.2	14.1
10	0.25	300	75	46.2	16.7	81.5	43.8
11	0.25	350	50	45.9	16.8	98.7	33.8
12	0.25	250	100	39.5*	19.7*	72.2	24.4
13	0.4	350	75	51.8	19.7	60.0	48.5
14	0.4	300	50	57.2	15.9	83.0	39.1
15	0.25	300	75	42.9	17.5	96.3	30.7

* Only 100 particles counted.

Table 3
Correlation factor of operating parameters on average particle size.

Operating parameter	Correlation factor on average particle size
Concentration	0.893
Temperature	0.054
Flow rate	−0.036

3. Results and discussion

3.1. Effect of operating parameters and their interactions on APS

Correlation factors were determined for each parameter, identifying their significance on the APS. As shown in Table 3, the concentration was found to majorly influence particle size, with the temperature and flow rate having a lesser, almost insignificant effect. The effect of increased concentration on the APS is illustrated through the TEM images in Fig. 3. Using the Stat Ease software, the contribution percentage of each parameter and parameter interaction was analysed on the resulting APS, as depicted in Fig. 4. A graphical representation of these trends are also displayed in Fig. 5a and b.

A model to predict the APS was also derived through the factorial trial and is presented in Eq. (2). This model can be used to predict the average particle size within the range of the factorial trial, by substituting the values of A, B and C within their −1 to 1 range as shown in Table 1:

$$\begin{aligned}\text{APS} = {} & 44.00 + (9.29 * \text{A}) + (0.56 * \text{B}) + (-0.37 * \text{C}) + (2.38 * \text{AB}) \\ & + (0.90 * \text{AC}) + (1.25 * \text{BC}) + (1.16 * \text{A}^2) \\ & + (-0.037 * \text{B}^2) + (-0.013 * \text{C}^2) \end{aligned} \quad (2)$$

3.1.1. Effect of the interaction between concentration and temperature on APS

The interaction between concentration and reaction temperature were found to have the largest interaction effect on APS, with a 12.1% contribution factor as depicted in Fig. 4. This interaction was related to both parameters having a large effect on the level of supersaturation and growth kinetics. Higher concentrations result in higher numbers of ferric ions in solution, while an increase in temperature decreases the solubility of the salt solution under supercritical conditions, increases reaction rates and promotes the dehydration step [4,15]. Although these occurrences both increase the degree of supersaturation, the key perhaps lies in the diffusion coefficient. Xu [4] further stated that the diffusion coefficient was found to increase as the reaction temperature approached the supercritical region, where an increased diffusion coefficient has been linked to an increase in dominant crystal size [16]. Therefore it has been proposed that when the rate of diffusion and number of ions in solution are both high, rapid particle growth is promoted as shown in Fig. 5a and b.

Using the factorial trial model for APS (Eq. (2)), accurate predictions were made at various combinations of concentration and temperature at constant flow. It can be shown from Fig. 6 that the effect of temperature is highly dependent on the concentration of the precursor solution. At a 0.1 M concentration, the APS was found to decrease linearly from 40.2 nm down to 34 nm as the temperature increased. Yet at a 0.25 M concentration, the effect of temperature on APS was found to have little effect. The APS was found to gradually decrease from 45 nm to 43.6 nm at 0.25 M. While at 0.4 M, the APS was found to increase in linearly from 52 nm to 55.6 nm. This revealed that under different concentrations, an increase in temperature may appear to show an increase in APS (0.4 M), it may be shown to have negligible effect

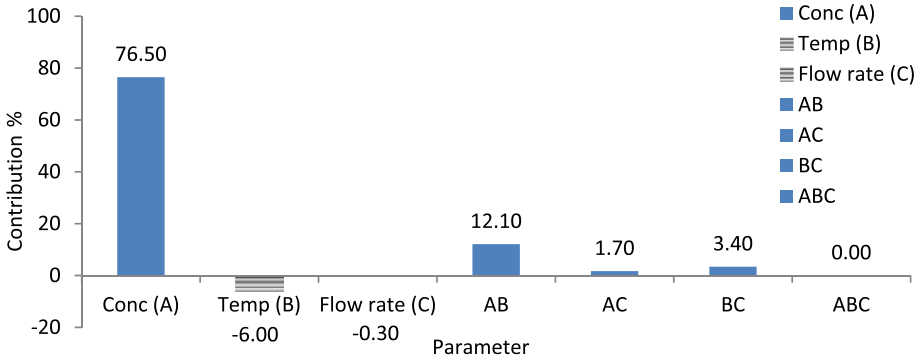

Fig. 4. Contribution percentage and interaction of operating parameters on the resulting APS.

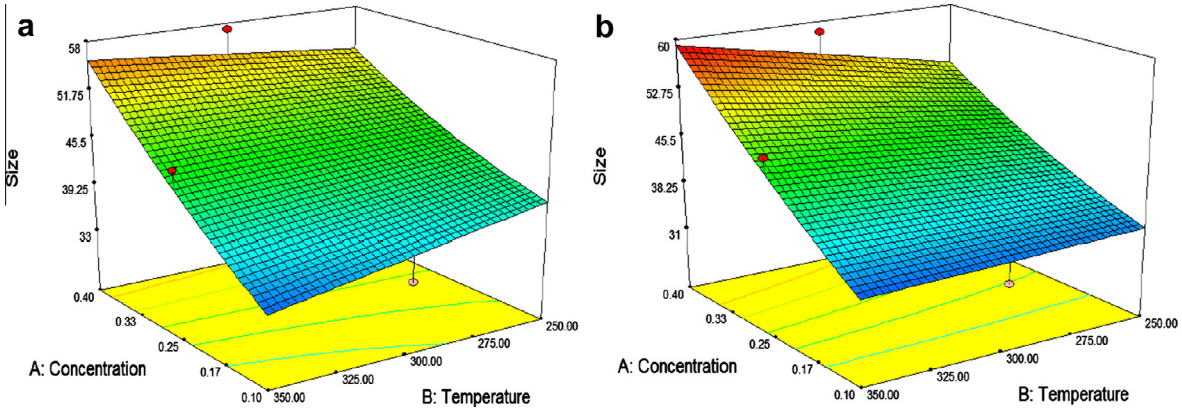

Fig. 5. 3D quadratic plot of concentration versus temperature on the effect on particle size at (a) low flow rate – 50 ml/min and (b) high flow rate – 100 ml/min.

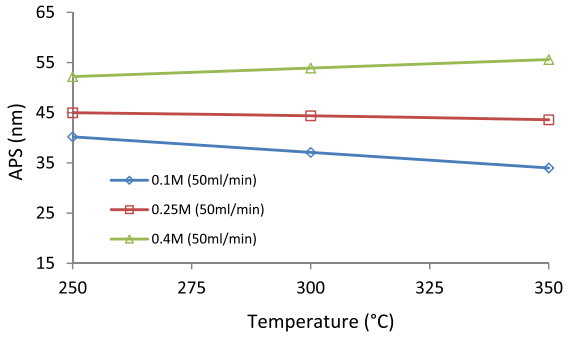

Fig. 6. Prediction of the effect of temperature on APS at varied concentrations and 50 ml/min flow rate.

Table 4
Correlation factor of operating parameters on particle size distribution (CV).

Operating parameter	Correlation factor on particle size distribution (CV)
Concentration	0.030
Temperature	−0.235
Flow rate	0.545

on average particle size (0.25 M) or it may take on a downward trend or show a decrease in APS (0.1 M).

It was therefore proposed that the effect of temperature on APS is highly sensitive to concentration, which may be responsible for the conflicting reports and confusion in the literature. The same trends were observed even when the flow rate and hence residence time was varied, showing that the effect of temperature on APS was only influenced by the concentration of the precursor solution.

3.2. Effect of operating parameters and the effect of their interactions on PSD

The particle size distribution is most effectively analysed through the coefficient of variation (CV), which is a relationship between the standard deviation and the APS. As depicted in Table 4, the PSD was found to be majorly influenced by the flow rate, where increased flow rates increased the CV. Temperature was also found to have a small yet significant effect on reducing the CV, while the concentration was evident to have negligible effect on the CV. The effect of flow rate on the PSD is illustrated by the frequency plots in Fig. 7. The percentage contribution of parameters and parameter interactions are depicted in Fig. 8, indicating which combinations of parameters play which role on the resulting PSD. These interactions can also be observed by analysing Fig. 9a and b.

A model to predict the PSD was also derived through the factorial trial as shown in Eq. (3). This model can be used to predict the CV value within the range of the factorial trial, by substituting the values of A, B and C within their −1 to 1 range as shown in Table 1:

$$CV = 18.77 + (0.14 * A) + (-1.14 * B) + (2.45 * C) + (0.75 * AB) + (0.87 * AC) + (-0.63 * BC) + (2.39 * A^2) + (1.14 * B^2) + (-2.28 * C^2) \quad (3)$$

3.2.1. Effect of the interaction between concentration and flow rate on PSD

Although the effect of concentration by itself was insignificant, when coupled with flow rate it largely influenced the PSD, with a contribution factor of 22.1%, as depicted in Fig. 5. Using the factorial trial model predictions (Eq. (3)), the CV percentage was

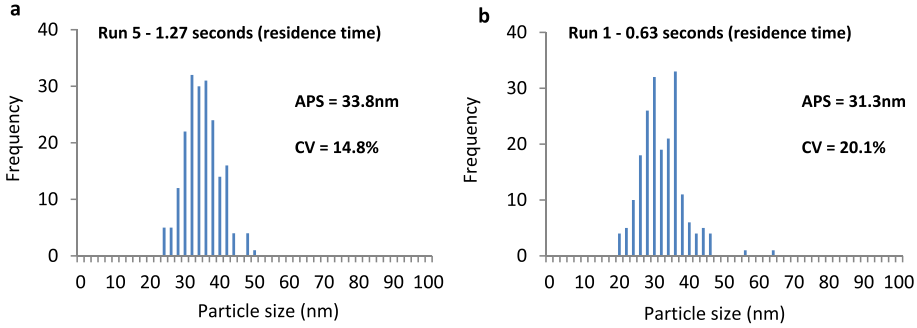

Fig. 7. Effect of flow rate on the PSD curve at a constant 0.1 M and 300 °C (a) Run 5–50 ml/min and (b) Run 1–100 ml/min.

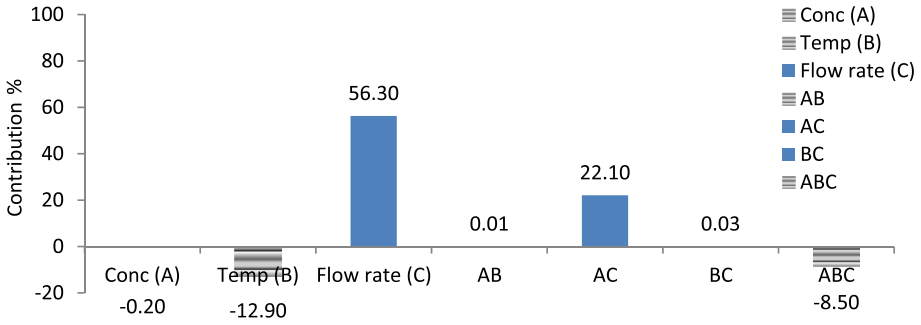

Fig. 8. Contribution percentage and interaction of operating parameters on the resulting PSD.

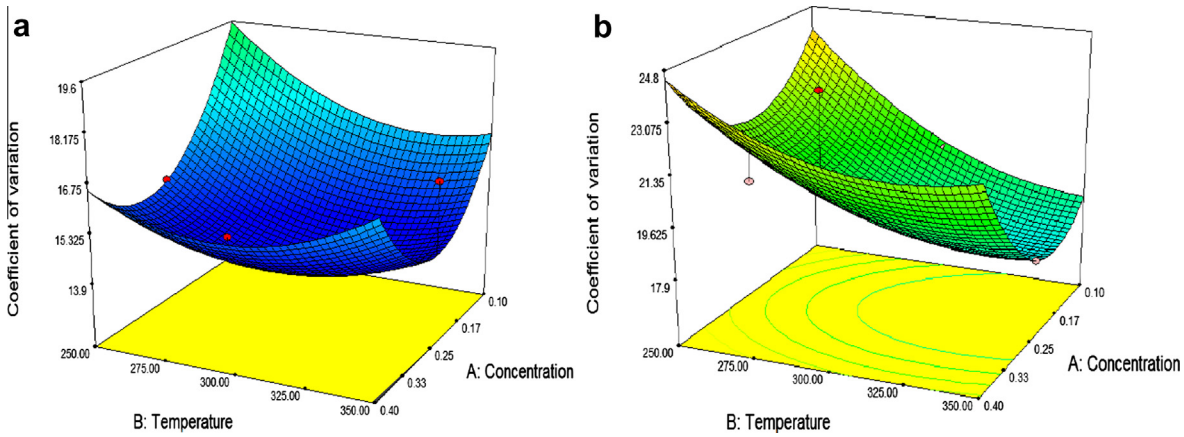

Fig. 9. 3D quadratic plot of concentration versus temperature on the effect on PSD at (a) low flow rate – 50 ml/min and (b) high flow rate – 100 ml/min.

Table 5
Correlation factor of operating parameters on product yield.

Operating parameter	Correlation factor on product yield
Concentration	0.504
Temperature	0.557
Flow rate	0.132

predicted and plotted versus flow rate at different concentrations, as depicted in Fig. 10.

Fig. 10 shows how different trends occur as the flow rate and concentration were varied at a constant reaction temperature of 300 °C. When comparing high concentrations (green line) and low concentrations (blue line) at 100 ml/min flow rate, at high concentrations there was insufficient time for the reaction of all Fe^{3+} ions in solution - resulting in a higher CV value. In contrary, at low concentrations (0.1 M), the short reaction time was able to convert a higher percentage of Fe^{3+} ions to form particles, leading to a lower CV value. As the flow rate decreased, the increase in residence time allowed more time for particle growth. As it has been proposed that particle growth occurs via OR kinetics in CHS [9], higher residence times allowed for a narrower PSD at all concentrations. At higher concentrations, as the monomers decomposed in solution, the remaining Fe^{3+} ions in solution were able to attach onto the newly formed particles through surface nucleation. Therefore as shown in Fig. 10, as the residence time increased, higher concentrations favoured a decrease in CV value through secondary growth or surface nucleation. This was in agreement with the gradient of CV decrease between 50 and 75 ml/min in Fig. 10, where it was calculated that 0.4 M had the steepest gradient (0.224), which decreased as the concentration dropped to 0.25 M (0.189) and 0.1 M (0.154). The middle concentration, 0.25 M, was

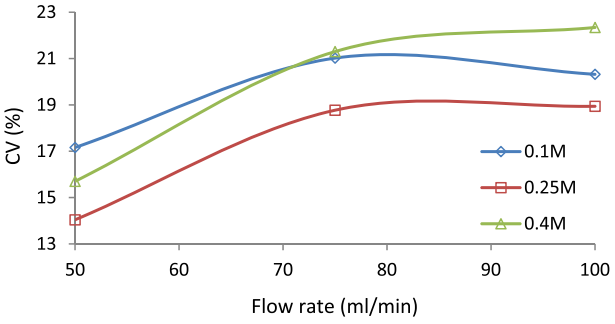

Fig. 10. Effect of CV versus flow rate at different concentrations and at a constant temperature of 300 °C.

also found to have the lowest CV value at all flow rates tested in this study. Although this was unexpected, it was noted that the slightly higher concentration had a stronger driving force for particle nucleation and growth [17]. A concentration of 0.25 M was optimal for obtaining a narrow PSD in the flow rate range studied, which was attributed to supersaturation rates high enough to induce rapid nucleation but a concentration low enough for sufficient Fe^{3+} ions to react and nucleate uniformly in the relatively short residence times calculated for this study.

3.3. Effect of operating parameters and their effect on PY

As depicted in Table 5, the product yield was found to be majorly influenced by the concentration and the temperature and an increase in each parameter led to increase in PY. The flow rate was also found to have a small increasing effect on PY. The

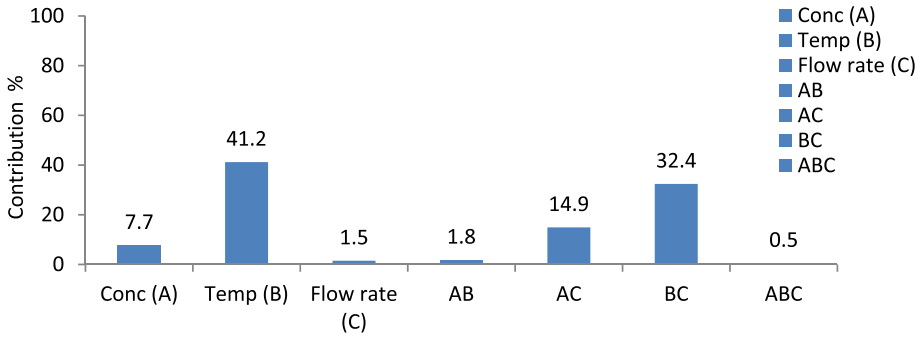

Fig. 11. Contribution percentage and interaction of operating parameters on the resulting PY.

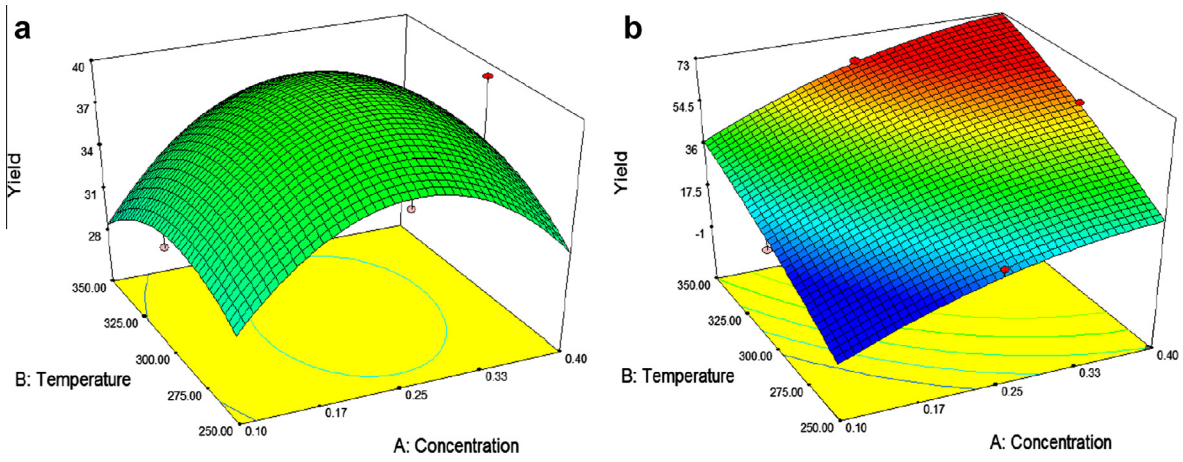

Fig. 12. 3D quadratic plot of concentration versus temperature on the effect on product yield at (a) low flow rate – 50 ml/min and (b) high flow rate – 100 ml/min.

percentage contribution of parameters and parameter interactions on the resulting PSD are shown in Fig. 11, with all combinations leading to an increase in PY. These interactions can also be observed by analysing Fig. 12a and b.

A model to predict the product yield was also derived through the factorial trial and is given in Eq. (4). This model can be used to predict the product yield percentage within the range of the factorial trial, by substituting the values of A, B and C within their −1 to 1 range as shown in Table 1:

$$PY = 39.67 + (8.91 * A) + (9.85 * B) + (2.34 * C) + (0.78 * AB) + (7.65 * AC) + (10.02 * BC) + (-6.23 * A^2) + (-2.91 * B^2) + (2.37 * C^2) \quad (4)$$

3.3.1. Effect of the interaction between concentration and flow rate on PY

A significant interaction was observed between the concentration and the flow rate with a significant 14.9% contribution factor, attributed to the combination of high levels of supersaturation associated with a higher concentration [15] and efficient mixing at higher flow rates [18]. Although the residence time decreased drastically with an increase in flow rate, it was proposed that more particles precipitated at high concentrations due to the increased mixing turbulence when compared with the increased residence times associated with lower flow rates. Therefore the high degree of supersaturation and turbulence led to nearly instantaneous nucleation of almost all Fe^{3+} ions in solution, and therefore the effect of increased residence time yielded little secondary nucleation. The relationship between the concentration and flow rate at a constant 300 °C temperature is represented by Fig. 13, which uses PY predictions from the PY factorial trial model Eq. (4).

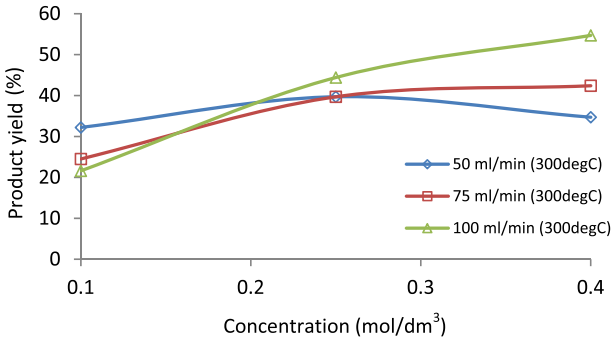

Fig. 13. Effect of product yield versus concentration at varied flow rate and constant temperature.

Fig. 13 conveys how at low concentrations, lower rates of flow (higher residence times) are required to maximise the PY. While at higher concentrations, increased flow rates (turbulent mixing) become more effective at inducing rapid nucleation and hence increased product yield.

3.3.2. Effect of the interaction between temperature and flow rate on PY

The temperature and flow rate were identified to have a critical interaction, with a contribution factor of 32.4%. Although the effect of flow rate alone was minimal, when combined with temperature it had a massive effect on the resulting PY. Using the factorial trial

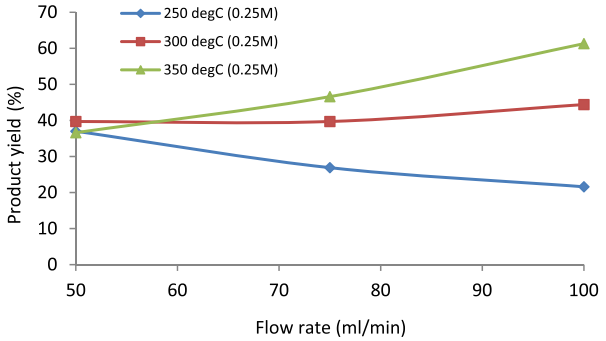

Fig. 14. Effect of product yield versus flow rate at varied temperature and constant 0.25 M concentration.

Table 6
Correlation factor of operating parameters on relative crystallinity.

Operating parameter	Correlation factor on relative crystallinity
Concentration	−0.483
Temperature	0.235
Flow rate	−0.589

model for PY (Eq. (4)), Fig. 14 represents PY predictions versus flow rate at varied temperature and at a constant 0.25 M concentration.

As shown in Fig. 14, the PY percentage was relatively constant at the lowest flow rate of 50 ml/min and across all temperatures, while as the flow rate increased 3 different trends were observed. At low temperatures (250°), the PY decreased as the flow rate increased, unlike at moderate temperatures (300 °C) where the PY increased gradually with increased flow. While at the highest temperature studied (350 °C), the PY was found to greatly increase with flow rate.

It was identified that at high temperatures and flow rates, the precursor solution tends to migrate higher up into the water line due to the excessive difference in density of the two streams [19]. Therefore the combination of high flow rate and high temperature effectively enhanced flow partitioning, channelling the precursor solution higher up the water line, theoretically increasing the reactor residence time. Mixing studies in tee mixers have also shown increased turbulence as the flow rate and the difference in densities between the two streams increases [20], thus more effective mixing is also promoted in turbulent zones during this interaction. Taking all factors into consideration, high temperatures and high flow rates provide an optimal environment for a high PY across all concentrations, by increasing the theoretical residence time, increasing mixing turbulence and promoting high nucleation and growth rates.

3.4. Effect of operating parameters and their effect on RC

As represented in Table 6, the degree of relative crystallinity was found to be heavily dependent on the concentration and the rate of flow, with a slightly lower dependence on temperature. The percentage contribution of parameters and parameter interactions on the resulting RC are shown in Fig. 15. These interactions can also be observed by analysing Fig. 16a and b.

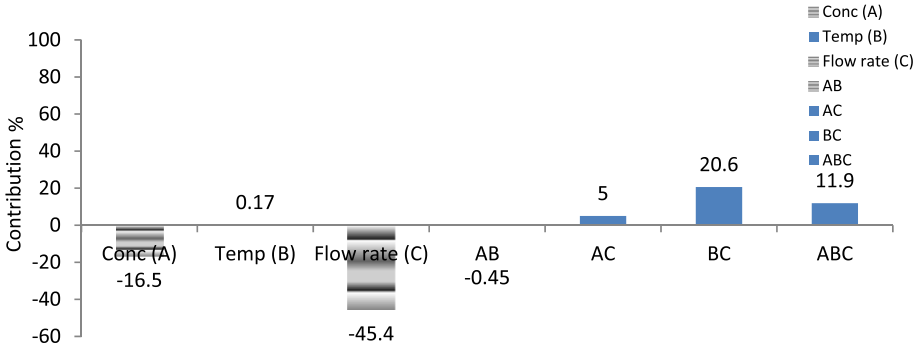

Fig. 15. Contribution percentage of operating parameters on the resulting relative crystallinity (Blue = positive effect; Red = negative effect). (For interpretation of the references to color in this figure legend, the reader is referred to the web version of this article.)

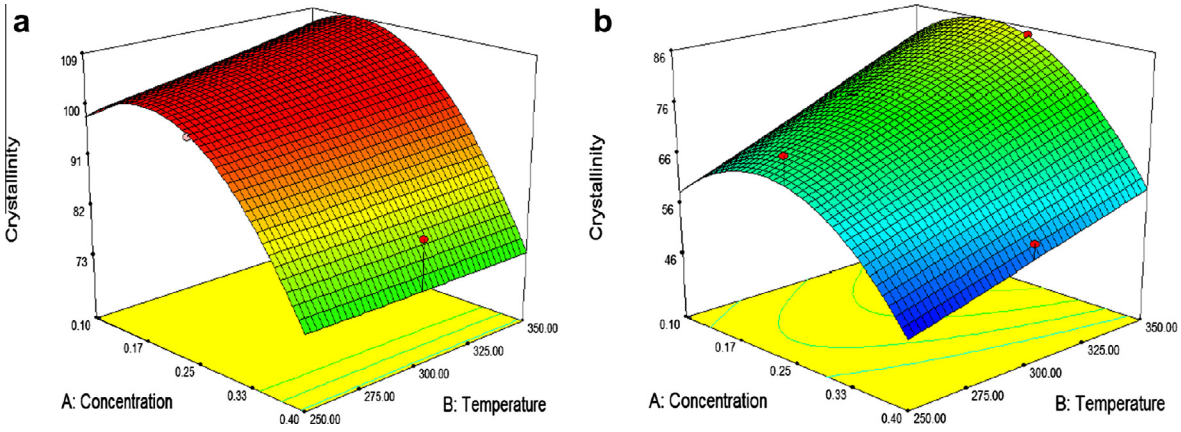

Fig. 16. 3D quadratic plot of concentration versus temperature on the effect on relative crystallinity at (a) low flow rate – 50 ml/min and (b) high flow rate – 100 ml/min.

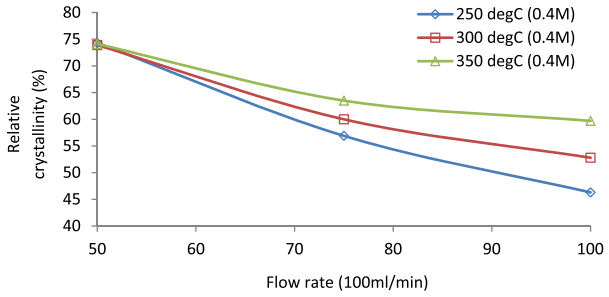

Fig. 17. Effect of flow rate on the resulting RC percentage at varied temperature and 0.4 M.

A model to predict the relative crystallinity was derived through the factorial trial and is depicted in Eq. (5.3). This model can be used to predict the RC value within the range of the factorial trial, by substituting the values of A, B and C within their −1 to 1 range as shown in Table 1:

$$\text{Relative crystallinity} = 85.33 + (-11.09 * A) + (5.40 * B) + (-13.51 * C) + (-2.10 * AB) + (2.93 * AC) + (3.40 * BC) + (-14.28 * A^2) + (0.15 * B^2) + (3.37 * C^2) \quad (5)$$

3.4.1. Effect of the interaction between temperature and flow rate on PY

A strong interaction between the temperature and flow rate was identified with a contribution factor of 20.6%, as indicated in Fig. 15. The factorial trial model for RC was used to plot the predicted RC percentage versus the flow rate at different temperatures and at a constant 0.4 M concentration, as depicted Fig. 17.

It was observed from Fig. 17, that at low flow rates (50 ml/min) the RC was almost identical across the high and low temperature variations used in this study. However as the flow rate increased, the resulting RC was found to decrease proportionately with a decrease in temperature. Temperature is also a function of residence time, which decreases slightly as the temperature increases [12]. Yet as mentioned in Section 3.3.2, high flow rates and temperatures can promote enhanced flow partitioning, forcing the precursor solution up the waterline, increasing the residence time. It is apparent that at a flow rate of 100 ml/min, this interaction led to an increase in residence time as the temperature increased, overpowering the predicted decrease in residence time at higher temperatures [12]. This increase in residence time increased the reaction period, allowing more time for crystallographic arrangement under the high temperature conditions.

3.5. Effect of operating parameters and parameter interactions on particle characteristics

The effects of all process parameters and parameter interactions on particle characteristics have been summarized in Table 7. When looking at the system as a whole, the concentration was found to be the critical parameter, having extremely strong influences on all particle characteristics apart from the PSD. The interaction between the concentration and temperature was found to be responsible for the conflicting reports on the effect of temperature on APS in the literature. The effect of temperature on APS was found to be sensitive to concentration, with different trends occurring. The interaction between temperature and flow rate proved to be an effective method of increasing PY and RC, at little expensive of altering the APS or PSD, offering promise for increasing the process efficiency.

4. Conclusion

Controlling particle growth through the manipulation of process parameters is vital for the commercialization and upscale of the CHS process, however achieving this is troublesome. The system is intricate and complex, and attempting to control one particle characteristic often leads to altering others. Through the factorial trial, process parameters and parameter interactions have been evaluated and the critical parameters for particle control were identified as follows:

- For control of APS: concentration, and the interaction between temperature and concentration.
- For control of PSD: Flow rate, and the interaction between flow rate and concentration.
- For control of PY: Temperature; concentration; the interaction between concentration and flow rate, and the interaction between temperature and flow rate.
- For control of RC: Temperature; concentration; the interaction between flow rate and temperature, and the interaction between all three operating parameters. The RC was complex to control and is highly dependent on all three operating parameters.

Certain operating parameters appeared to have little effect on a specific particle characteristic such as the effect of flow rate on PY, yet interacted strongly with other parameters.

It was shown that the interaction between concentration and temperature caused a significant increase in APS, thus providing a plausible explanation for the conflicting reports the effects of temperature on APS in CHS.

The critical process parameters for maximum product yield and high crystallinity with minimum effect on average particle size and size distribution was found to be the interaction between

Table 7
Summary of process parameter and parameter interactions on particle characteristics.

Parameter	Average particle size	Particle size distribution	Product yield	Relative crystallinity
Concentration	Critical increase (0.893)	Negligible (0.03)	Major increase (0.504)	Moderate decrease (−0.483)
Temperature	Negligible (0.054)	Minor decrease (−0.235)	Major increase (0.557)	Minor increase (0.235)
Flow rate	Negligible (−0.036)	Major increase (0.545)	Minor increase (0.132)	Major decrease (−0.589)
Interactions				
Concentration and Temperature	Significant increase (12.1%)	Negligible (0.01%)	Very minor increase (1.8%)	Negligible (−0.45%)
Concentration and Flow rate	Very minor increase (1.7%)	Major increase (22.1%)	Significant increase (14.9%)	Minor increase (5%)
Temperature and Flow rate	Minor increase (3.4%)	Negligible (0.03%)	Critical increase (32.4%)	Major increase (20.6%)
All three parameters	Negligible (0%)	Moderate decrease (−8.5%)	Negligible (0.5%)	Significant increase (11.9%)

Correlation factor scale: <0.1 = negligible, 0.1–0.3 = minor, 0.2–0.5 = moderate, 0.5–0.75 = major, >0.75 = critical.
Contribution factor scale: <1% = negligible, 1–3% = very minor, 3–5% = minor, 5–10% = moderate, 10–20% = significant, 20–30% = major, >30% = critical.

temperature and flow rate and could be the key for successful upscaling of the CHS process.

Acknowledgments

Financial support for this work was provided by the South African NRF Research Infrastructure Support Programme (RISP), Grant Number UID: 78697 and Cape Peninsula University of Technology.

References

[1] S. Mandal, A.H. Muller, Facile route to the synthesis of porous alpha-Fe_2O_3 nanorods, Mater. Chem. Phys. 111 (2008) 438–443.
[2] L.P. Zhu, G.H. Liao, N.C. Bing, X. Zhao, Synthesis of monodisperse shuttle-like alpha-Fe_2O_3 nanorods via the EDA-assisted method, Matter. Lett. 65 (2011) 1287–1290.
[3] A.S. Teja, P.Y. Koh, Synthesis, properties, and applications of magnetic iron oxide nanoparticles, Prog. Cryst. Growth Charact. Mater. 55 (2009) 22–45.
[4] C. Xu, Continuous and batch hydrothermal synthesis of metal oxide nanoparticles and metal oxide-activated carbon nanocomposites (Unpublished Ph.D. thesis), Georgia Institute of Technology, USA, Georgia, 2006.
[5] Y. Hao, A. Teja, Continuous hydrothermal crystallization of a-Fe_2O_3 and Co_3O_4 nanoparticles, J. Mater. Res. 18 (2003) 415–422.
[6] C. Xu, A.S. Teja, Continuous hydrothermal synthesis of iron oxide and PVA-protected iron oxide nanoparticles, J. Supercrit. Fluids 44 (2008) 85–91.
[7] Y. Hakuta, K. Seino, H. Ura, T. Adschiri, K. Arai, Production of ultra-fine ceria particles by hydrothermal synthesis under supercritical conditions, J. Mater. Sci. 17 (1998) 1211–1213.
[8] S.I. Kawasaki, K. Sue, R. Ookawara, Y. Wakashima, Engineering study of continuous supercritical hydrothermal method using a T-shaped mixer: Experimental synthesis of NiO nanoparticles and CFD simulation, J. Supercrit. Fluids 54 (2010) 96–102.
[9] M.T. Liang, S.H. Wang, Y.L. Chang, H.I. Hsiang, H.J. Huang, M.H. Tsai, W.C. Juan, S.F. Lu, Iron oxide synthesis using a continuous hydrothermal and solvothermal system, Ceram. Int. 36 (2010) 1131–1135.
[10] T. Noguchi, K. Matsui, N.M. Islam, Y. Hakuta, H. Hayashi, Rapid synthesis of alpha-Al_2O_3 nanoparticles in supercritical water by continuous hydrothermal flow reaction system, J. Supercrit. Fluids 46 (2008) 129–136.
[11] K. Sue, S.I. Kawasaki, M. Suzuki, Y. Hakuta, H. Hayashi, K. Arai, Y. Takebayashi, S. Yoda, T. Furuya, Continuous hydrothermal synthesis of Fe_2O_3, NiO, and CuO nanoparticles by superrapid heating using a T-type micro mixer at 673 K and 30 MPa, Chem. Eng. J. 166 (2011) 947–953.
[12] L.J. Cote, A.S. Teja, A.P. Wilkinson, Z.J. Zhang, Continuous hydrothermal synthesis of $CoFe_2O_4$ nanoparticles, Fluid Phase Equilib. 210 (2003) 307–317.
[13] A. Aimable, B. Xin, N. Millot, D. Aymes, Synthesis of zeolite a from calcined diatomaceous clay: optimization studies, J. Solid State Chem. 181 (2008) 183–189.
[14] B. Gosh, D. Agrawal, S. Bhatia, Synthesis of zeolite a from calcined diatomaceous clay: optimization studies, Ind. Eng. Chem. Res. 33 (1994) 2107–2110.
[15] G. Demopoulos, Aqueous precipitation and crystallization for the production of particulate solids with desired properties, Hydrometallurgy 96 (2009) 199–214.
[16] R. Cahn, P. Haasen, E. Cremer, Materials Science Technology: Phase Transformations in Materials, fifth ed., WCH Press, Weiheim, 1991.
[17] K. Sue, M. Suzuki, K. Arai, T. Ohashi, H. Ura, K. Matsui, Y. Hakuta, H. Hayashi, M. Watanabe, T. Hiaki, Size-controlled synthesis of metal oxide nanoparticles with a flow-through supercritical water method, Green Chem. 8 (2006) 634–638.
[18] J. Sierra-Pallares, D.L. Marchiso, E. Alanso, M.T. Parra-Santos, F. Castro, M.J. Cocero, Quantification of mixing efficiency in turbulent supercritical water hydrothermal reactors, Chem. Eng. Sci. 66 (2011) 1576–1589.
[19] P.J. Blood, J.P. Denyer, B.J. Azzopardi, M. Poliakoff, E. Lester, A versatile flow visualisation technique for quantifying mixing in a binary system: application to continuous supercritical water hydrothermal synthesis (SWHS), Chem. Eng. Sci. 59 (2004) 2853–2861.
[20] E. Lester, P. Blood, J. Denyer, D. Giddings, B. Azzopardi, M. Poliakoff, Reaction engineering: the supercritical water hydrothermal synthesis of nano-particles, J. Supercrit. Fluids 37 (2006) 209–214.